Genomic binding dynamics of PBAF are regulated via select chromatin states

Charles A. Kenworthy[1], Vincent Wong[1], Patrycja Dziuba[1], Luke D. Lavis[2], Wei-Li Liu[1], Robert H. Singer[1,2], and Robert A. Coleman[1*]

[1]Gruss-Lipper Biophotonics Center, Department of Anatomy and Structural Biology, Albert Einstein College of Medicine, Bronx, New York 10461, USA

[2]Janelia Research Campus, Howard Hughes Medical Institute, Ashburn, Virginia, 20147

*To whom correspondence should be addressed.
Gruss-Lipper Biophotonics Center, Department of Anatomy and Structural Biology, Albert Einstein College of Medicine, Bronx, NY 10461 Tel: 718-430-8623; Email: robert.coleman2@einstein.yu.edu

Running Title: PBAF chromatin binding dynamics

Keywords: PBAF, chromatin remodeling, Histone acetylation, Histone H3.3, Single Molecule Tracking, bromodomain.

Abstract

ATP-dependent chromatin-remodeling complexes such as PBAF mediate changes in chromatin structure, leading to regulation of transcriptional bursting. PBAF is targeted to genomic loci by histone acetylation. Despite extensive in vitro studies, how these chromatin remodelers rapidly bind and discriminate genomic targets in vivo remains unclear. Therefore, we sought to understand how the PBAF complex interacts with different chromatin states using live-cell single molecule fluorescence microscopy. Dual color tracking revealed that PBAF binds H3.3 marked chromatin within actively transcribed regions for faster time periods relative to binding to HP1α containing heterochromatin. Notably, elevation of histone acetylation levels increased the frequency of PBAF revisiting to genomic foci as defined by clustered binding. Furthermore, deletion of six bromodomains within the BAF180 subunit of PBAF reduced chromatin target search efficiency, clustered binding activity, and anchoring to the genome. These findings suggest that acetyl-lysine dependent clustered binding of PBAF to select genomic loci may facilitate rapid chromatin remodeling in actively transcribed regions. Our work also indicates that the dynamics of PBAF mediated chromatin state alterations proceed at fast timescales that may fine-tune transcription regulation.

Introduction

Transcription occurs in a series of stochastic bursts interspersed with periods of inactivity (Larson et al. 2011; Sanchez and Golding 2013; Senecal et al. 2014). It is generally thought that ATP-dependent chromatin remodelers alter chromatin structure to regulate the dynamics of transcriptional bursting (Metivier et al. 2003; Raser and O'Shea 2004; Tirosh and Barkai 2008; Tirosh et al. 2009; Sanchez et al. 2013). ATP-dependent chromatin remodelers are localized to actively transcribing loci via bromodomains that recognize specific acetyl-lysine residues in histones (Xue et al. 2000; Lemon et al. 2001; Ferreira et al. 2007; Mujtaba et al. 2007; Filippakopoulos et al. 2012). The repeated targeting of ATP-dependent chromatin remodelers to acetylated chromatin likely plays a key role in destabilizing arrays of nucleosomes in transcriptionally active regions (Jenuwein and Allis 2001; Boeger et al. 2003; Boeger et al. 2004; Parnell et al. 2008; Lorch et al. 2011; Musladin et al. 2014; Marathe et al. 2017). At enhancers and promoters, dynamic incorporation of histone variants, such as H3.3, and histone acetylation can also directly destabilize nucleosomes to potentially regulate transcriptional bursting (Hebbes and Allen 2000; Jin and Felsenfeld 2007; Sun et al. 2007; Henikoff et al. 2009; Jin et al. 2009; Calo and Wysocka 2013). After chromatin is remodeled, the promoter becomes permissive to transcription. Recent single molecule studies revealed that RNA Polymerase II (Pol II) is rapidly loaded onto the promoter every 4-8 seconds forming convoys of Pol II lasting for minutes (Tantale et al. 2016). Whether the rapid kinetics of transcription initiation necessitates chromatin remodeling on fast time-scales of seconds remains unclear. Despite years of detailed in vitro studies, it is unknown how chromatin-

remodeling enzymes dynamically target and regulate changes to chromatin structure in vivo.

PBAF is a large multisubunit mammalian ATP-dependent chromatin-remodeling complex that mobilizes and/or evicts nucleosomes to regulate key cellular processes, including transcription, DNA repair, and replication (Xue et al. 2000; Lemon et al. 2001; Kakarougkas et al. 2014). Prior biochemical and imaging studies have demonstrated that bromodomains within PBAF and its yeast counterpart RSC increase their affinity for chromatin (VanDemark et al. 2007; Wang et al. 2012; Duan and Smerdon 2014; Philpott et al. 2014; Porter and Dykhuizen 2017). The majority of bromodomains within PBAF (6 out of 8) are located in the BAF180 subunit (Brownlee et al. 2012). It is likely that BAF180 uses these six bromodomains to facilitate PBAF's localization to a large number of differentially acetylated genomic loci including regions at enhancers and the 5' and 3' end of genes (Yen et al. 2012; Zhu et al. 2015). Despite several studies showing that mutation of BAF180 is a driver for clear cell renal carcinoma (Varela et al. 2011; Cancer Genome Atlas Research 2013), it is unknown how BAF180 directs PBAF's chromatin binding activity. Therefore understanding the role of the BAF180 bromodomains in recognition of acetylated genomic loci is important for the knowledge of eukaryotic transcriptional regulation.

Once bound to chromatin, PBAF and RSC have been implicated in both activation and repression of transcription (Cairns et al. 1996; Lemon et al. 2001; Damelin et al. 2002; Van de Vosse et al. 2013; Kakarougkas et al. 2014; Nichol et al. 2016). PBAF is thought to evict nucleosomes from enhancers and promoters to potentiate transcription (Kim et al. 2009; Yen et al. 2012; Krietenstein et al. 2016; Marathe et al. 2017). In

support of this model, in vivo conditional knockout of RSC leads to rapid nucleosome accumulation throughout highly transcribed genes (Parnell et al. 2008). In addition, PBAF represses transcription of genes surrounding sites of DNA damage (Kakarougkas et al. 2014). It is currently unknown how PBAF's activity differs during activation versus repression of transcription.

Previous in vitro studies have suggested that chromatin remodelers (e.g. PBAF and RSC) utilize differing enzyme kinetics for sliding versus eviction of nucleosomes (Whitehouse et al. 1999; Boeger et al. 2003; Bruno et al. 2003; Boeger et al. 2004; Lorch et al. 2006; Lorch et al. 2011; Musladin et al. 2014; Clapier et al. 2016; Clapier et al. 2017). At high DNA translocation efficiencies, RSC rapidly slides and ejects nucleosomes, which likely occurs during activation of transcription. Inefficient DNA translocation leads to slow nucleosome sliding without eviction (Clapier et al. 2016). Given that nucleosome eviction is unlikely compatible with repression, it is possible that PBAF and RSC reposition nucleosomes via sliding to inhibit transcription factor binding and transcription initiation.

Thus far, previous in vivo and in vitro work has provided different estimates for kinetic rates of chromatin-remodeling. In vitro studies suggest that chromatin remodelers require at least 10s of seconds to remodel nucleosomes (Zhang et al. 2006; Harada et al. 2016). However, in vivo FRAP studies indicate that chromatin remodelers interact with chromatin on the order of a few seconds (Phair et al. 2004; Johnson et al. 2008; Erdel et al. 2010; Erdel and Rippe 2012; Philpott et al. 2014). The varied time scales of heterogenous interactions of remodelers with chromatin's different states are poorly defined. Therefore, it is important to characterize chromatin-remodeler function at high

temporal and spatial resolution in vivo. Single molecule imaging can address these questions by measuring chromatin remodeling dynamics within the complex milieu of the nucleus.

Accelerated progress in live-cell single-molecule tracking (SMT) techniques has been achieved in both microscopy and fluorescent dyes (Chen et al. 2014; Izeddin et al. 2014; Liu et al. 2014; Grimm et al. 2015; Knight et al. 2015; Coleman et al. 2016; Zhen et al. 2016). These advances have permitted direct in-vivo tracking of individual nuclear factors with unprecedented spatial and temporal resolution. In addition, with the improved photochemical properties of dyes, continuous imaging of single-molecule dynamics across an entire nucleus for seconds to minutes can be accomplished. SMT also allows for classification of PBAF populations displaying heterogeneous chromatin binding interactions. Armed with this advanced tool, we characterized PBAF's interaction with chromatin in live cells via SMT of fluorescently tagged BAF180 subunit within PBAF. We found that PBAF transiently and non-specifically probed chromatin on sub-second timescales. Upon stable binding to chromatin in cells, PBAF remained engaged for ~14 seconds on average, consistent with in vitro measurements (Zhang et al. 2006). Deletion of BAF180 bromodomains decreased the percentage of stable binding events and PBAF's residence time on chromatin. Furthermore, PBAF binds to large chromatin domains in distinct subnuclear regions with different kinetics. We assessed PBAF binding activity within H3.3 (actively transcribing) versus HP1α (repressed) marked chromatin. Intriguingly, the results show that PBAF binds H3.3 regions for significantly less time than HP1α marked areas, consistent with high ATP-dependent nucleosome turnover within transcriptionally active regions. Furthermore, stimulation of

histone acetylation primarily leads to increased genomic localization and repeated binding of PBAF within small subnuclear foci as defined by clustered binding. Deletion of BAF180 bromodomains reduces PBAF's clustered binding in foci. Overall, our study demonstrates how PBAF genomic localization and binding dynamics are regulated via bromodomain-acetyl-lysine interactions and select chromatin states.

Results

PBAF chromatin binding dynamics via Single Molecule Tracking in vivo.

To characterize the dynamic binding of PBAF to chromatin *in vivo*, we generated a stable U2-OS cell line expressing Halo- and flag-tagged human BAF180 (Halo-fBAF180) (Supplemental Figure S1A). Expression was confirmed through *in vivo* labeling of Halo-fBAF180 using a membrane permeable dye (JF549 conjugated Halo-Tag Ligand [JF549HTL]) (Grimm et al. 2015) followed by SDS-PAGE (Supplementary Figure S1B). Halo-fBAF180 is overexpressed ~1.7-fold compared to control cell lines containing the Halo-tag alone via Western blotting using an antibody against BAF180 (Supplementary Figure S1C). Incorporation of Halo-fBAF180 into the PBAF complex was further confirmed by immunoprecipitation via the flag-tag followed by western blotting against the BRG1 subunit (Supplementary Figure S1D).

Live cell Single Molecule Tracking (SMT) was then performed using HILO microscopy (Chen et al. 2014) to image JF549HTL-labeled Halo-fBAF180 in cells. To detect PBAF molecules stably bound to chromatin, we utilized camera exposures of 500 ms (Figure 1A and Supplemental Movie). Fast-diffusing molecules cannot be resolved as single particles and are blurred out at this long exposure time. Single PBAF molecules, stably bound to chromatin targets, appear as distinct Point Spread Functions (PSFs) that can be spatially and temporally resolved (Figure 1A). Multiple Target Tracking (MTT) algorithms (Serge et al. 2008) were applied to determine chromatin-binding activity of single PBAF molecules over time throughout the nucleus (Figure 1B). Single molecules of Halo-fBAF180 within individual frames of a movie were first localized through 2D Gaussian fitting. Chromatin-binding events were defined as a track by linking single

BAF180 molecules in successive frames whose positions remained in a highly confined area based on expected diffusion constants (panel i). Each chromatin-binding event was mapped by averaging the position of all individual localizations within the entire track (panel i, red X). On average, 19,287 PBAF chromatin-binding events were localized in each live cell during ~18 minutes of continuous imaging (panels ii and iii). The residence time of PBAF bound to chromatin was defined as the length in seconds of individual binding events (Figure 1C). Chromatin-binding dynamics of PBAF were then quantitatively evaluated by using a single and a two-component exponential distribution model to fit a histogram of residence times (Figure 1D)(Chen et al. 2014). A single exponential model yielded poor fits with ~2.3 second residence time, which was similar to values obtained with FRAP (Philpott et al. 2014; Gerstenberger et al. 2016). Fitting the residence time histograms with a double exponential function yielded two chromatin-binding populations of PBAF (Figure 1D). The predominant PBAF population (~86% of molecules) bound chromatin transiently with a residence time of ~0.8 seconds. This transient binding population likely represents non-specific scanning of PBAF along the genome based upon a previous live-cell SMT study on the Sox2 transcriptional activator (Chen et al. 2014). The remaining PBAF molecules (~14%) bound chromatin stably with an average residence time of ~13.9 seconds (Figure 1E). Importantly, photobleaching rates occurred with a $t_{1/2}$ of approximately 100-200 seconds indicating that we are likely measuring PBAF's dissociation from chromatin.

To validate that we were measuring genomic binding of the PBAF complex instead of unincorporated BAF180, we conducted fast diffusion experiments by imaging Halo-fBAF180 using short camera exposure times (effective exposure time = 25 ms) (Figure

S2). Halo-fBAF180 diffusion coefficients (D_{coeff}), based on individual trajectories, for a majority of freely diffusing molecules (~83%) were significantly slower (0.1-2μm^2/sec) than values from a of comparable protein complex with a molecular weight similar to BAF180 alone (3-5μm^2/sec) (Figure S2) (Schmidt et al. 2016). This suggests that the majority of our measured chromatin binding events arose from Halo-fBAF180 incorporated into a high molecular weight PBAF complex.

Multiple PBAF subunits, including BAF180, BRG1 and BRD7, contain bromodomains that recognize acetyl-lysine residues in chromatin (Charlop-Powers et al. 2010; Ho and Crabtree 2010; Brownlee et al. 2012; Filippakopoulos et al. 2012). BAF180 contains six bromodomains while BRG1 and BRD7 each contain one bromodomain, suggesting a potential major role of BAF180 in PBAF's genomic targeting. To determine the contribution of bromodomains to PBAF binding, we deleted the six bromodomains within BAF180 (i.e. ΔBD) (Supplemental Figure S1A). Removal of BAF180 bromodomains resulted in a decrease in both the residence time (Figure 1E) and the proportion of molecules stably bound to chromatin (Supplemental Figure S3). This suggests that BAF180 bromodomains affect both the association and dissociation of PBAF with chromatin targets.

A previous study documented that histone acetylation helps to stabilize binding of ATP-chromatin remodelers to chromatin templates (Hassan et al. 2001). Therefore, we examined if increased levels of acetylation affect PBAF binding to chromatin. Thus, Halo-fBAF180 cells were pre-incubated with a histone deacetylase inhibitor (SAHA) for 24 hours prior to imaging. Western blot analysis confirmed a ~4-fold increase of histone acetylation with SAHA treatment (Supplemental Figure S4). Interestingly, no changes in

residence time (Figure 1E) or in the proportion of PBAF molecules stably binding to chromatin (Supplemental Figure S3) were observed upon SAHA treatment. These results suggest that increased histone acetylation doesn't globally change PBAF's chromatin-binding association or dissociation kinetics.

Mapping high-frequency PBAF binding in subnuclear regions

In human cells, chromosomes form subcompartments containing a large number of co-regulated genes within TADs or transcription factories (Nora et al. 2012; Cisse et al. 2013; Buckley and Lis 2014). Therefore, we hypothesized that PBAF may be acting to remodel chromatin over large spans of the genome within spatially distinct regions in the nucleus. Thus, we developed an approach to define PBAF binding density with the nucleus (Figure 2). Binding density heat maps were generated by counting the number of PBAF-chromatin binding events (binding events/μm^2/sec) in a given window as it was raster scanned across the nucleus one pixel at a time (Figure 2A, left panel). Spatially isolated subcompartments representing high frequency PBAF binding over large genomic regions were scattered throughout the nucleus (Figure 2A, right panel). The results show that PBAF is likely remodeling chromatin over large but select genomic regions that are packaged in confined subcompartments. Subnuclear regions depleted of PBAF binding likely represent large regions of the genome containing a chromatin state that is somehow refractive to remodeling by PBAF.

Previous studies have revealed varied histone acetylation patterns in large contiguous regions throughout the genome (Bulger 2005; Wang et al. 2008). Therefore it is possible that PBAF could differentially bind chromatin containing diverse sets of histone acetylation marks within individual subcompartments. To determine if different

subcompartments served as diverse chromatin binding targets, we determined the residence time for PBAF molecules collectively bound within individual subnuclear regions (Figure 2B). PBAF that was stably bound to chromatin within different subcompartments had residence times that varied from ~2.8-42.9 seconds (Figures 2C, and data not shown). We also observed a large degree of variability in the percentage of PBAF stably bound to chromatin (Supplemental Figure S5A). In contrast, there was minimal variation in the residence time amongst the different subcompartments for the PBAF population that transiently bound to chromatin (Supplemental Figure S5B). These data suggest individual subcompartments may contain large regions of differentially encoded histone marks that bind PBAF.

To better understand the diversity of PBAF's chromatin binding activity within different subnuclear regions, we generated a histogram of residence times collected from all subcompartments (Figure 3A). Our analysis revealed a dominant population of subcompartments where PBAF exhibited an average residence time of ~11.0 seconds with a significant tail towards longer-lived interactions (Figure 3A, green curve). This observation implies that there are at least two different types of subcompartments recognized by PBAF.

To test if PBAF was recognizing these subcompartments via histone acetylation marks, we performed a similar analysis on our BAF180 bromodomain deletion (Halo-fBAF180-ΔBD). A histogram of Halo-fBAF180-ΔBD residence times within different subcompartments showed a significant decrease in PBAF's residence time on chromatin compared to wild-type BAF180 (Figure 3A, red curve). Interestingly, Halo-fBAF180-ΔBD residence time in different subnuclear regions is even shorter than the global

average time (Figure 3A, red curve versus Figure 1E). This finding indicates that PBAF's bromodomains may play a more important role binding within large distinct chromatin domains.

To find out whether increased acetylation affects PBAF within these subcompartments, we inhibited histone deacetylation with SAHA in our Halo-fBAF180 cells (Figure 3B). We observed a slightly elevated residence time of PBAF on chromatin in the subcompartments (Figure 3B, brown curve). Collectively, these findings suggest PBAF targets distinct pools of genomic loci in large subcompartments throughout different subnuclear regions. Furthermore, PBAF's interaction with these target loci over large genomic spans can be regulated via bromodomain and acetyl-lysine interactions with chromatin.

PBAF interaction dynamics in euchromatic versus heterochromatic regions

We next sought to determine how PBAF-chromatin binding activity changes in euchromatin versus heterochromatin. To differentially localize euchromatin and heterochromatin within the cell, we conducted two-color SMT imaging with PBAF using Halo-fBAF180WT and either SNAP tagged H3.3 (H3.3-SNAP) or HP1α (SNAP-HP1α). SMT traces of H3.3-SNAP or SNAP-HP1α were analyzed and used to generate high density H3.3 or HP1α subcompartments within cells (Figures 4A top left and Supplemental Figure S6). PBAF SMT trajectories from the same cells were masked using these H3.3 or HP1α subcompartments (Figure 4A bottom and Supplemental Figure S6 bottom). 1-CDF plots of PBAF residence times mapped within H3.3 or HP1α subcompartments were fitted to a double-exponential function. PBAF that localized within H3.3 marked subcompartments bound for a shorter duration than tracks that

localized within HP1α regions (Figure 4B). These results suggested that PBAF rapidly remodels chromatin associated with actively transcribing genes compared to repressed heterochromatin.

Bromodomain-dependent clustering of PBAF bound to chromatin in small foci

Our previous analysis (Figure 2) mapped high frequency PBAF binding to large genomic regions likely containing co-regulated genes. However, this low-resolution analysis was unable to define repeated PBAF binding to small genomic regions, including enhancers and promoters (Yen et al. 2012; Marathe et al. 2017). Therefore we performed high-resolution clustering analysis to define small foci (~250nm) of repeated PBAF/chromatin binding events lasting at least 2 seconds (Figure 5B). Further filtering revealed small foci of repeated PBAF/chromatin binding events lasting longer than 12 seconds (Figure 5C, left panel). Importantly, no clustering was detected in simulations where localizations of an equivalent number of binding events were randomized throughout the nucleus (Figure 5C, right panel). These results are consistent with previous studies showing the clustered binding of Sox2 and RNA Polymerase II at enhancers and promoters in nuclear domains less than 250 nm (Cisse et al. 2013; Liu et al. 2014; Ricci et al. 2015). Therefore, we speculate that these PBAF foci represent repeated binding to individual nucleosomes in small genomic regions at enhancers and promoters.

We aimed to understand how PBAF cluster formation was influenced by acetylated histone/bromodomain interactions. To quantitatively define PBAF clustering, we compared the number of small foci detected with the total number of PBAF binding events in each cell. This analysis revealed a linear relationship between the number of small foci detected and the number of PBAF binding events in each cell (Figure 6A).

This linear relationship allowed comparison of PBAF clustering between individual cells expressing either Halo-fBAF180WT or Halo-fBAF180-ΔBD (Figure 6A). Deletion of the bromodomains within BAF180 led to significant deficits in PBAF clustering when filtering for binding durations as low as 2 seconds (Figure 6A). These bromodomain-dependent differences in cluster formation were maintained when filtering for longer binding durations (Figure 6B). This result suggests that PBAF's repeated targeting to individual nucleosomes is likely dependent on BAF180 bromodomains. Accordingly, increased histone acetylation resulted in a greater number of PBAF clusters formed at thresholds of 8 and 12-seconds relative to DMSO treatment (Figures 6D and E). Interestingly, increased histone acetylation via SAHA treatment did not affect Halo-fBAF180WT PBAF clustering at a 2-second event threshold (Figure 6C). This suggests that increased histone acetylation preferentially leads to repeated long-lived PBAF binding at an increased number of genomic loci. Taken together, bromodomain-acetyl-lysine interactions function to both increase targeting and anchoring of PBAF to select genomic loci.

Discussion

PBAF utilizes BAF180 bromodomains for targeting and anchoring to chromatin in vivo.

Our live cell SPT assays reveal that PBAF/BAF180 dynamically samples the genome via a series of brief interactions (<1 second) in search of chromatin targets (Figure 1D). Removal of BAF180's bromodomains decreases the search efficiency (Figure S3) resulting in a higher percentage of transient unstable interactions with chromatin. These findings are consistent with previous studies indicating that bromodomains enhance association of remodeling complexes with chromatin (Hassan et al. 2002; Philpott et al. 2014; Porter and Dykhuizen 2017). Once PBAF/BAF180 finds its target, it remains bound to chromatin for ~14 seconds on average throughout the nucleus. Strikingly, deletion of BAF180's bromodomains enhances dissociation of PBAF from chromatin (residence time of ~10 seconds-ΔBD vs 14 seconds-WT) (Figure 1E). Collectively, our results indicate that BAF180 bromodomains regulate both genomic localization and anchoring of PBAF to chromatin (Figure 7A).

PBAF heterogeneously binds large chromatin domains in discrete subnuclear regions

A large body of work now indicates that transcriptionally co-regulated genes are clustered in subcompartments containing TADs or transcription factories in the nucleus (Nora et al. 2012; Cisse et al. 2013; Buckley and Lis 2014). Therefore, we speculated that PBAF would need to remodel chromatin over large spans of the genome in unique subnuclear compartments. Indeed, our heat maps indicated high frequency PBAF/chromatin binding in large discrete subnuclear regions. PBAF primarily displayed a residence time of ~11 seconds within these large subcompartments (Figures 2 and 3A).

However, there were a significant number (~20%) of subcompartments where PBAFs residence time was greater than 15 seconds. This indicates potentially at least two different types of chromatin domains targeted by PBAF. The identities of the different types of chromatin domains are unknown. However, we speculate that these large chromatin domains contain multiple co-regulated genes that must be remodeled by PBAF during transcription, replication or DNA repair (Xue et al. 2000; Lemon et al. 2001; Kakarougkas et al. 2014). Disruption of BAF180 bromodomains reduced PBAF's residence time within these large subnuclear regions to approximately 8 seconds (Figure 3A). Thus PBAF binding in these large subcompartments is likely regulated by bromodomains that anchor the complex to acetylated nucleosomes.

PBAF exhibits shorter chromatin binding interactions within euchromatic versus heterochromatic regions

Previous studies documented that actively transcribing genes in euchromatin display dynamic chromatin incorporation and turnover of H3.3 relative to heterochromatic regions (Deaton et al. 2016). In addition, in vitro experiments revealed that H3.3-containing nucleosomes are particularly sensitive to salt and therefore inherently unstable (Jin and Felsenfeld 2007; Henikoff et al. 2009; Jin et al. 2009). Therefore, it is likely that chromatin remodelers would require less time to remodel and evict H3.3-containing nucleosomes than heterochromatin lacking H3.3. Our imaging experiments revealed that PBAF displayed shorter residence times in H3.3 marked actively transcribing regions compared to HP1α containing heterochromatic regions (Figures 4B and 7B). Therefore rapid turnover of PBAF's genomic occupancy in actively

transcribing regions could be the direct result of nucleosome stability, which may define different chromatin states.

Nucleosomes in actively transcribing euchromatin contain histone post-translational modifications within the histone globular region that favor destabilization or eviction of nucleosomes (Ahmad and Henikoff 2002; Di Cerbo et al. 2014; Bowman and Poirier 2015; Deaton et al. 2016; Pradhan et al. 2016). This may also contribute to the short-lived PBAF residence times observed in H3.3-rich nuclear regions. Strikingly however, most PBAF binding events still occur outside of H3.3-rich regions and thus are not in areas of active transcription. PBAF localization to these stable nucleosomes could be related to other roles outside of active transcription such as repression, DNA repair, and specification of pericentromeric or subtelomeric regions (Ferreira et al. 2011; Verdaasdonk et al. 2012; Van de Vosse et al. 2013; Kakarougkas et al. 2014).

Clustered binding of PBAF to small genomic regions is dependent on bromodomains

Interestingly, PBAF displays dynamic repeated binding to chromatin in small foci (~250nm) (Figure 5). These binding foci may be related to PBAF's localization to nucleosomes in enhancers and promoters where PBAF may remodel chromatin during multiple rounds of transcriptional bursts (Yen et al. 2012; Marathe et al. 2017). The number of these PBAF binding foci decreases upon deletion of BAF180's bromodomains (Figure 6A). Correspondingly, the number of binding foci (i.e. clusters) containing repeated long-lived PBAF chromatin binding events increases upon inhibition of histone deacetylation (SAHA treatment, Figures 6B and 7A). This suggests that SAHA treatment may lead to a greater number of acetylated nucleosomes throughout the genome. However this potential increase in acetylated nucleosomes at select sites does not shift

the global chromatin binding characteristics of PBAF (Figures 1E and S4). This finding is consistent with previous work showing promoter specific effects on transcription upon inhibition of histone deacetylase activity (Huang et al. 2014; Rafehi et al. 2014; Vleeshouwer-Neumann et al. 2015). Overall, we envision that histone deacetylation reduces both targeting of PBAF to chromatin and the duration of stable binding at specific genomic loci in vivo (Figure 7A).

Orchestrating PBAF's chromatin binding, nucleosome remodeling, and transcriptional bursting

PBAF and RSC are thought to remodel nucleosomes via DNA translocation (Velankar et al. 1999; Zhang et al. 2006; Clapier et al. 2016; Clapier et al. 2017). Interestingly, in vitro single molecule studies on RSC have revealed that the average duration for nucleosomal DNA translocation is ~10 seconds (Zhang et al. 2006). Roughly equivalent timescales between in vitro DNA translocation and in vivo chromatin residence time that we observe (~11-14 seconds, Figures 1E and 3A), suggests that we may be visualizing nucleosome remodeling in our live-cell single molecule studies. However our imaging experiments in this study cannot determine if PBAF is evicting or sliding nucleosomes. Future work on high-resolution live-cell two color imaging of PBAF bound to fluorescently tagged nucleosomes will help delineate these possibilities.

Notably, PBAF's residence time on chromatin is highly similar to activators (Sox2 and p53, ~15 seconds (Chen et al. 2014; Coleman et al. 2017)) and the Polycomb repressor (Cbx7, ~7 seconds (Zhen et al. 2016)) as measured using single molecule tracking. This further indicates that a variety of transcription factors dynamically access their chromatin targets on timescales of seconds. RNA Pol II recruitment and promoter

escape also occurs approximately every 4-8 seconds during transcriptional bursts (Tantale et al. 2016). Furthermore, transcriptional bursting may be controlled by changes in chromatin structure. Collectively, the fast dynamics of transcriptional bursts likely necessitates rapid binding and unbinding of transcriptional regulators such as chromatin remodelers, activators, and repressors.

Over the last 50 years numerous research groups have uncovered a plethora of histone post-translational marks (PTMs) utilized by chromatin remodelers to regulate transcription activation (Verdin and Ott 2015). Genomic studies have mapped these histone acetylation marks to broad chromatin domains along with select regions of promoters and enhancers (Bulger 2005; Roh et al. 2005; Wang et al. 2008). Recent studies on 3D organization of the genome have revealed subcompartments containing histone marks associated with activated transcription (Nora et al. 2012; Bonev and Cavalli 2016). By examining the dynamic genomic binding of PBAF, which recognizes many of these acetylation marks, our study helps to define spatial and temporal histone modification of subcompartments. In the future, live-cell single molecule imaging of additional histone PTM writers, readers, and the histone marks themselves will aid in spatiotemporal characterization of the 4D epigenome.

Materials and Methods

Plasmid constructions and biochemistry

Details of plasmid construction and biochemical analysis of Halo-BAF180 can be found in the supplemental methods section.

Cell Culture and generation of FRT site, Halo-tag, Halo-fBAF180WT, Halo-fBAF180WT/SNAP-HP1α, and Halo-fBAF180WT/H3.3-SNAP stable cell lines

U2-OS cells were grown in complete DMEM (high glucose DMEM supplemented with 10% FBS, 2 mM Glutamax (Fisher Scientific), 100 I.U./mL Penicillin, and 100 μg/mL Streptomycin (Corning)). To create U2-OS cells containing a single FRT site for future generation of isogenic cell lines, we transiently transfected cells with pFRT/lacZeo plasmid containing an FRT site (Invitrogen). Single cell colonies were selected in 300 μg/mL zeocin. To create the Halo-tag or Halo-fBAF180WT cell lines, pFRT-Halo or pFRT-Halo-fBAF180WT plasmids were co-transfected with pOG44 plasmid into U2-OS-FRT cells. Selection for Halo-tag or Halo-fBAF180WT stably expressing cells was performed by supplementing media with 75-150 μg/mL Hygromycin b. To create Halo-fBAF180WT/SNAP-HP1α or Halo-fBAF180WT/H3.3-SNAP stable cells lines, cells stably expressing Halo-fBAF180WT were co-transfected with pSNAP-HP1α or pSNAP-H3.3 plasmids together with a second plasmid containing puromycin resistance. Cells expressing Halo-fBAF180WT along with SNAP-HP1α or H3.3-SNAP were selected using puromycin.

Live-cell fluorescent labeling of Halo-fBAF180 WT and Halo-fBAF180-ΔBD in U2-OS cells

Cells stably expressing Halo-fBAF180WT were plated on 35 mm MatTek imaging dishes 2-3 days before imaging in selective media so that on the day of imaging, there would be ~$5x10^5$ cells/imaging dish. In the case of Halo-fBAF180-ΔBD, 24 hours prior to transfection, parental U2-OS cell were plated in 35mm MatTek imaging dishes at a density of $5x10^4$ cells/imaging dish. Cells were then transiently transfected with the pFRT-Halo-BAF180-ΔBD plasmid 17-20 hours later. Following transfection, cells were incubated overnight.

24 hours before labeling, cells were treated with either 2.5 μM SAHA or matching vehicle control (DMSO 0.25% final volume) and were incubated at 37°C with 5% CO_2. Immediately prior to imaging, cells were incubated with 0.4 nM JF549-HTL for 15 minutes at 37°C with 5% CO_2. Cells were then washed 3x with 1x PBS and placed in complete DMEM and incubated for 30 minutes at 37°C with 5% CO_2. Cells were then washed 2x with 1x PBS and placed in L-15 imaging media + 10% FBS for imaging. All labeling and imaging was conducted in the presence of either 2.5 μM SAHA or DMSO.

Dual color live-cell fluorescent labeling of Halo-fBAF180WT and SNAP-HP1α or H3.3-SNAP in U2-OS cells

Cells stably expressing Halo-fBAF180WT and either SNAP-HP1 or H3.3-SNAP were plated on 35 mm MatTek imaging dishes in selective media 1-3 days before imaging so that on the day of imaging, there would be ~$5x10^5$ cells/imaging dish. Immediately prior to imaging, cells were incubated at 37°C with 5% CO_2 with 10nM SNAP-Cell 647-SiR (New England Biolabs) and 0.4nm JF549-HTL for a total of 30 and 15 minutes respectively. Cells were then washed 3x with 1x PBS and placed in complete

DMEM and incubated for 30 minutes at 37°C with 5% CO_2. Cells were then washed 2x with 1x PBS and placed in L-15 imaging media + 10% FBS for imaging.

Live-cell single molecule imaging of Halo-fBAF180WT, SNAP-HP1α or H3.3-SNAP in U2-OS cells

All imaging sessions were carried out at room temperature. Samples were continuously illuminated using a 532nm (13 W/cm^2, Coherent) or 640nm (9.5 W/cm^2, Coherent) laser. Time-lapse two dimensional images of single molecules were acquired with a customized inverted Nikon Eclipse Ti microscope with a 100x oil-immersion objective lens (Nikon, 1.49NA) and further magnified 1.5x post-objective. BAF180 images were acquired at 2Hz for ~18 minutes using an EMCCD (iXon, Andor) with a 512 x 512 pixel field of view (final pixel size of 84nm). SNAP imaging proceeded at 2Hz for ~4.5 minutes in cells that also expressed either H3.3-SNAP or SNAP-HP1α.

Image Processing and single particle tracking

Acquired images were processed to subtract background and subjected to Multi-Target Tracking (MTT) to resolve the trajectories of individual molecules (Serge et al. 2008) using custom MATLAB scripts.

Determination of BAF180 chromatin binding residence times

Each cell had the nucleus masked based on boundaries of the strong nuclear BAF180 signal and confirmed via imaging using white light. Tracks that fell outside of the nucleus were excluded. Photobleach rates were then determined for each background-subtracted movie. Track-length was plotted as a 1-Cumulative Density Function (1-CDF).

Single- and double-exponential models were then fitted to these 1-CDF functions to determine the residence times.

Global comparisons of stable residence times (>1 second) and proportions of molecules participating in stable residence events were conducted by taking the global stable residence time and the proportion of molecules participating in stable residence events for each cell. One-way ANOVA followed by Tukey's post-hoc t-tests were then performed to determine pairwise significance.

Mapping of PBAF binding subcompartments

Contiguous areas of high PBAF binding density in cells were determined by 1-pixel raster scanning of an 18x18 pixel window across cells. Binding events that fell within these windows were then counted to provide an overall binding density for individual pixels throughout the nucleus. The resulting PBAF density map was then filtered so that pixels that displayed a binding density lower than the average global binding density were eliminated. Remaining areas were grouped as contiguous subcompartments and total event number was evaluated in each region. Subcompartments with fewer than 120 binding events were eliminated to make statistical analysis of events within regions more robust. Track lengths for particles within remaining subcompartments were then evaluated as 1-CDF functions and were fit to single- and double-exponential functions.

Specific binding components for each subcompartment were plotted as Probability Density Functions (PDF) based on genotype or treatment condition. Statistical differences between treatment groups were then assessed using a two-sample Kolmogorov-Smirnov test.

Determination of territorial binding dynamics for PBAF within HP1α or H3.3 sucompartments

High binding density HP1α or H3.3 subcompartments were mapped using MTT and raster scanning as described above. Remaining subcompartments were then filtered so that regions below a threshold of 0.5% of total cellular binding events for HP1α or H3.3 were eliminated. PBAF binding events within individual HP1α or H3.3 subcompartments were then examined. Regions containing less than 120 PBAF binding events were eliminated. 1-CDF plots of PBAF binding event residence times within individual remaining subcompartments were fitted with single- and double-exponential functions. Comparisons between PBAF populations localizing within particular subcompartments were made using a two-sample Kolmogorov-Smirnov test.

Analysis of PBAF clustering

Event density maps were taken and rendered at a pixel size of 8.4 nm before being 1 pixel raster scanned across the nucleus with an octagon of 168 nm in diameter. Octagon widows centered on an individual pixel containing 3 PBAF binding events were considered clusters. Further filtering was conducted based on duration of binding events lasting at least 0, 1, 2, 4, 6, 8, 10, 12, 14, or 16 seconds. For each condition, cluster number per cell was then plotted against total track number. The slope and R^2-value of the resulting regression line was calculated in each condition. Simulations were performed using randomized positions of nuclear tracks followed by clustering analysis.

Acknowledgements

We thank Y.J. Chen and C.S. Peng for development of initial Matlab scripts used for SPT tracking. We are grateful to Z. Liu for providing the Matlab script and technical advice for analysis of diffusion rates. We thank S. Healton for reagents and technical assistance in acid extraction of histones, and J.C. Wheat for providing SAHA reagent and initial aliquots of acetyl-H3 antibody. We also thank D. Shechter for providing histone H3 antibody. This work was supported by a grant from the NIH/NIBIB (1U01EB021236-03, RAC and RHS) and a NIH Medical Scientist Training Program Grant (T32GM007288, CAK).

References

Ahmad K, Henikoff S. 2002. The histone variant H3.3 marks active chromatin by replication-independent nucleosome assembly. *Mol Cell* **9**: 1191-1200.

Boeger H, Griesenbeck J, Strattan JS, Kornberg RD. 2003. Nucleosomes unfold completely at a transcriptionally active promoter. *Molecular cell* **11**: 1587-1598.

Boeger H, Griesenbeck J, Strattan JS, Kornberg RD. 2004. Removal of promoter nucleosomes by disassembly rather than sliding in vivo. *Molecular cell* **14**: 667-673.

Bonev B, Cavalli G. 2016. Organization and function of the 3D genome. *Nature reviews Genetics* **17**: 661-678.

Bowman GD, Poirier MG. 2015. Post-translational modifications of histones that influence nucleosome dynamics. *Chem Rev* **115**: 2274-2295.

Brownlee PM, Chambers AL, Oliver AW, Downs JA. 2012. Cancer and the bromodomains of BAF180. *Biochem Soc Trans* **40**: 364-369.

Bruno M, Flaus A, Stockdale C, Rencurel C, Ferreira H, Owen-Hughes T. 2003. Histone H2A/H2B dimer exchange by ATP-dependent chromatin remodeling activities. *Mol Cell* **12**: 1599-1606.

Buckley MS, Lis JT. 2014. Imaging RNA Polymerase II transcription sites in living cells. *Current opinion in genetics & development* **25**: 126-130.

Bulger M. 2005. Hyperacetylated chromatin domains: lessons from heterochromatin. *The Journal of biological chemistry* **280**: 21689-21692.

Cairns BR, Lorch Y, Li Y, Zhang M, Lacomis L, Erdjument-Bromage H, Tempst P, Du J, Laurent B, Kornberg RD. 1996. RSC, an essential, abundant chromatin-remodeling complex. *Cell* **87**: 1249-1260.

Calo E, Wysocka J. 2013. Modification of enhancer chromatin: what, how, and why? *Mol Cell* **49**: 825-837.

Cancer Genome Atlas Research N. 2013. Comprehensive molecular characterization of clear cell renal cell carcinoma. *Nature* **499**: 43-49.

Charlop-Powers Z, Zeng L, Zhang Q, Zhou MM. 2010. Structural insights into selective histone H3 recognition by the human Polybromo bromodomain 2. *Cell Res* **20**: 529-538.

Chen J, Zhang Z, Li L, Chen BC, Revyakin A, Hajj B, Legant W, Dahan M, Lionnet T, Betzig E et al. 2014. Single-molecule dynamics of enhanceosome assembly in embryonic stem cells. *Cell* **156**: 1274-1285.

Cisse, II, Izeddin I, Causse SZ, Boudarene L, Senecal A, Muresan L, Dugast-Darzacq C, Hajj B, Dahan M, Darzacq X. 2013. Real-time dynamics of RNA polymerase II clustering in live human cells. *Science (New York, NY)* **341**: 664-667.

Clapier CR, Iwasa J, Cairns BR, Peterson CL. 2017. Mechanisms of action and regulation of ATP-dependent chromatin-remodelling complexes. *Nat Rev Mol Cell Biol*.

Clapier CR, Kasten MM, Parnell TJ, Viswanathan R, Szerlong H, Sirinakis G, Zhang Y, Cairns BR. 2016. Regulation of DNA Translocation Efficiency within the Chromatin Remodeler RSC/Sth1 Potentiates Nucleosome Sliding and Ejection. *Mol Cell* **62**: 453-461.

Coleman RA, Liu Z, Darzacq X, Tjian R, Singer RH, Lionnet T. 2016. Imaging Transcription: Past, Present, and Future. *Cold Spring Harbor symposia on quantitative biology*.

Coleman RA, Qiao Z, Singh SK, Peng CS, Cianfrocco M, Zhang Z, Piasecka A, Aldeborgh H, Basishvili G, Liu WL. 2017. p53 Dynamically Directs TFIID Assembly on Target Gene Promoters. *Molecular and cellular biology* **37**.

Damelin M, Simon I, Moy TI, Wilson B, Komili S, Tempst P, Roth FP, Young RA, Cairns BR, Silver PA. 2002. The genome-wide localization of Rsc9, a component of the RSC chromatin-remodeling complex, changes in response to stress. *Mol Cell* **9**: 563-573.

Deaton AM, Gomez-Rodriguez M, Mieczkowski J, Tolstorukov MY, Kundu S, Sadreyev RI, Jansen LE, Kingston RE. 2016. Enhancer regions show high histone H3.3 turnover that changes during differentiation. *Elife* **5**.

Di Cerbo V, Mohn F, Ryan DP, Montellier E, Kacem S, Tropberger P, Kallis E, Holzner M, Hoerner L, Feldmann A et al. 2014. Acetylation of histone H3 at lysine 64 regulates nucleosome dynamics and facilitates transcription. *Elife* **3**: e01632.

Duan MR, Smerdon MJ. 2014. Histone H3 lysine 14 (H3K14) acetylation facilitates DNA repair in a positioned nucleosome by stabilizing the binding of the chromatin Remodeler RSC (Remodels Structure of Chromatin). *The Journal of biological chemistry* **289**: 8353-8363.

Erdel F, Rippe K. 2012. Quantifying transient binding of ISWI chromatin remodelers in living cells by pixel-wise photobleaching profile evolution analysis. *Proc Natl Acad Sci U S A* **109**: E3221-3230.

Erdel F, Schubert T, Marth C, Langst G, Rippe K. 2010. Human ISWI chromatin-remodeling complexes sample nucleosomes via transient binding reactions and become immobilized at active sites. *Proc Natl Acad Sci U S A* **107**: 19873-19878.

Ferreira H, Flaus A, Owen-Hughes T. 2007. Histone modifications influence the action of Snf2 family remodelling enzymes by different mechanisms. *J Mol Biol* **374**: 563-579.

Ferreira ME, Flaherty K, Prochasson P. 2011. The Saccharomyces cerevisiae histone chaperone Rtt106 mediates the cell cycle recruitment of SWI/SNF and RSC to the HIR-dependent histone genes. *PLoS One* **6**: e21113.

Filippakopoulos P, Picaud S, Mangos M, Keates T, Lambert JP, Barsyte-Lovejoy D, Felletar I, Volkmer R, Muller S, Pawson T et al. 2012. Histone recognition and large-scale structural analysis of the human bromodomain family. *Cell* **149**: 214-231.

Gerstenberger BS, Trzupek JD, Tallant C, Fedorov O, Filippakopoulos P, Brennan PE, Fedele V, Martin S, Picaud S, Rogers C et al. 2016.

Identification of a Chemical Probe for Family VIII Bromodomains through Optimization of a Fragment Hit. *J Med Chem* **59**: 4800-4811.

Grimm JB, English BP, Chen J, Slaughter JP, Zhang Z, Revyakin A, Patel R, Macklin JJ, Normanno D, Singer RH et al. 2015. A general method to improve fluorophores for live-cell and single-molecule microscopy. *Nature methods* **12**: 244-250, 243 p following 250.

Harada BT, Hwang WL, Deindl S, Chatterjee N, Bartholomew B, Zhuang X. 2016. Stepwise nucleosome translocation by RSC remodeling complexes. *Elife* **5**.

Hassan AH, Neely KE, Workman JL. 2001. Histone acetyltransferase complexes stabilize swi/snf binding to promoter nucleosomes. *Cell* **104**: 817-827.

Hassan AH, Prochasson P, Neely KE, Galasinski SC, Chandy M, Carrozza MJ, Workman JL. 2002. Function and selectivity of bromodomains in anchoring chromatin-modifying complexes to promoter nucleosomes. *Cell* **111**: 369-379.

Hebbes TR, Allen SC. 2000. Multiple histone acetyltransferases are associated with a chicken erythrocyte chromatin fraction enriched in active genes. *J Biol Chem* **275**: 31347-31352.

Henikoff S, Henikoff JG, Sakai A, Loeb GB, Ahmad K. 2009. Genome-wide profiling of salt fractions maps physical properties of chromatin. *Genome Res* **19**: 460-469.

Ho L, Crabtree GR. 2010. Chromatin remodelling during development. *Nature* **463**: 474-484.

Huang J, Schriefer AE, Yang W, Cliften PF, Rudnick DA. 2014. Identification of an epigenetic signature of early mouse liver regeneration that is disrupted by Zn-HDAC inhibition. *Epigenetics* **9**: 1521-1531.

Izeddin I, Recamier V, Bosanac L, Cisse, II, Boudarene L, Dugast-Darzacq C, Proux F, Benichou O, Voituriez R, Bensaude O et al. 2014. Single-molecule tracking in live cells reveals distinct target-search strategies of transcription factors in the nucleus. *eLife* **3**.

Jenuwein T, Allis CD. 2001. Translating the histone code. *Science (New York, NY)* **293**: 1074-1080.

Jin C, Felsenfeld G. 2007. Nucleosome stability mediated by histone variants H3.3 and H2A.Z. *Genes Dev* **21**: 1519-1529.

Jin C, Zang C, Wei G, Cui K, Peng W, Zhao K, Felsenfeld G. 2009. H3.3/H2A.Z double variant-containing nucleosomes mark 'nucleosome-free regions' of active promoters and other regulatory regions. *Nat Genet* **41**: 941-945.

Johnson TA, Elbi C, Parekh BS, Hager GL, John S. 2008. Chromatin remodeling complexes interact dynamically with a glucocorticoid receptor-regulated promoter. *Mol Biol Cell* **19**: 3308-3322.

Kakarougkas A, Ismail A, Chambers AL, Riballo E, Herbert AD, Kunzel J, Lobrich M, Jeggo PA, Downs JA. 2014. Requirement for PBAF in transcriptional repression and repair at DNA breaks in actively transcribed regions of chromatin. *Mol Cell* **55**: 723-732.

Kim SI, Bresnick EH, Bultman SJ. 2009. BRG1 directly regulates nucleosome structure and chromatin looping of the alpha globin locus to activate transcription. *Nucleic Acids Res* **37**: 6019-6027.

Knight SC, Xie L, Deng W, Guglielmi B, Witkowsky LB, Bosanac L, Zhang ET, El Beheiry M, Masson JB, Dahan M et al. 2015. Dynamics of CRISPR-Cas9 genome interrogation in living cells. *Science (New York, NY)* **350**: 823-826.

Krietenstein N, Wal M, Watanabe S, Park B, Peterson CL, Pugh BF, Korber P. 2016. Genomic Nucleosome Organization Reconstituted with Pure Proteins. *Cell* **167**: 709-721 e712.

Larson DR, Zenklusen D, Wu B, Chao JA, Singer RH. 2011. Real-time observation of transcription initiation and elongation on an endogenous yeast gene. *Science (New York, NY)* **332**: 475-478.

Lemon B, Inouye C, King DS, Tjian R. 2001. Selectivity of chromatin-remodelling cofactors for ligand-activated transcription. *Nature* **414**: 924-928.

Liu Z, Legant WR, Chen BC, Li L, Grimm JB, Lavis LD, Betzig E, Tjian R. 2014. 3D imaging of Sox2 enhancer clusters in embryonic stem cells. *eLife* **3**: e04236.

Lorch Y, Griesenbeck J, Boeger H, Maier-Davis B, Kornberg RD. 2011. Selective removal of promoter nucleosomes by the RSC chromatin-remodeling complex. *Nat Struct Mol Biol* **18**: 881-885.

Lorch Y, Maier-Davis B, Kornberg RD. 2006. Chromatin remodeling by nucleosome disassembly in vitro. *Proc Natl Acad Sci U S A* **103**: 3090-3093.

Marathe HG, Watkins-Chow DE, Weider M, Hoffmann A, Mehta G, Trivedi A, Aras S, Basuroy T, Mehrotra A, Bennett DC et al. 2017. BRG1 interacts with SOX10 to establish the melanocyte lineage and to promote differentiation. *Nucleic acids research*.

Metivier R, Penot G, Hubner MR, Reid G, Brand H, Kos M, Gannon F. 2003. Estrogen receptor-alpha directs ordered, cyclical, and combinatorial recruitment of cofactors on a natural target promoter. *Cell* **115**: 751-763.

Mujtaba S, Zeng L, Zhou MM. 2007. Structure and acetyl-lysine recognition of the bromodomain. *Oncogene* **26**: 5521-5527.

Musladin S, Krietenstein N, Korber P, Barbaric S. 2014. The RSC chromatin remodeling complex has a crucial role in the complete remodeler set for yeast PHO5 promoter opening. *Nucleic Acids Res* **42**: 4270-4282.

Nichol JN, Galbraith MD, Kleinman CL, Espinosa JM, Miller WH, Jr. 2016. NPM and BRG1 Mediate Transcriptional Resistance to Retinoic Acid in Acute Promyelocytic Leukemia. *Cell Rep* **14**: 2938-2949.

Nora EP, Lajoie BR, Schulz EG, Giorgetti L, Okamoto I, Servant N, Piolot T, van Berkum NL, Meisig J, Sedat J et al. 2012. Spatial partitioning of the regulatory landscape of the X-inactivation centre. *Nature* **485**: 381-385.

Parnell TJ, Huff JT, Cairns BR. 2008. RSC regulates nucleosome positioning at Pol II genes and density at Pol III genes. *The EMBO journal* **27**: 100-110.

Phair RD, Scaffidi P, Elbi C, Vecerova J, Dey A, Ozato K, Brown DT, Hager G, Bustin M, Misteli T. 2004. Global nature of dynamic protein-chromatin interactions in vivo: three-dimensional genome scanning and dynamic interaction networks of chromatin proteins. *Mol Cell Biol* **24**: 6393-6402.

Philpott M, Rogers CM, Yapp C, Wells C, Lambert JP, Strain-Damerell C, Burgess-Brown NA, Gingras AC, Knapp S, Muller S. 2014. Assessing cellular efficacy of bromodomain inhibitors using fluorescence recovery after photobleaching. *Epigenetics Chromatin* **7**: 14.

Porter EG, Dykhuizen EC. 2017. Individual Bromodomains of Polybromo-1 Contribute to Chromatin Association and Tumor Suppression in Clear Cell Renal Carcinoma. *The Journal of biological chemistry* **292**: 2601-2610.

Pradhan SK, Su T, Yen L, Jacquet K, Huang C, Cote J, Kurdistani SK, Carey MF. 2016. EP400 Deposits H3.3 into Promoters and Enhancers during Gene Activation. *Mol Cell* **61**: 27-38.

Rafehi H, Balcerczyk A, Lunke S, Kaspi A, Ziemann M, Kn H, Okabe J, Khurana I, Ooi J, Khan AW et al. 2014. Vascular histone deacetylation by pharmacological HDAC inhibition. *Genome Res* **24**: 1271-1284.

Raser JM, O'Shea EK. 2004. Control of stochasticity in eukaryotic gene expression. *Science* **304**: 1811-1814.

Ricci MA, Manzo C, Garcia-Parajo MF, Lakadamyali M, Cosma MP. 2015. Chromatin fibers are formed by heterogeneous groups of nucleosomes in vivo. *Cell* **160**: 1145-1158.

Roh TY, Cuddapah S, Zhao K. 2005. Active chromatin domains are defined by acetylation islands revealed by genome-wide mapping. *Genes & development* **19**: 542-552.

Sanchez A, Choubey S, Kondev J. 2013. Regulation of noise in gene expression. *Annu Rev Biophys* **42**: 469-491.

Sanchez A, Golding I. 2013. Genetic determinants and cellular constraints in noisy gene expression. *Science* **342**: 1188-1193.

Schmidt JC, Zaug AJ, Cech TR. 2016. Live Cell Imaging Reveals the Dynamics of Telomerase Recruitment to Telomeres. *Cell* **166**: 1188-1197 e1189.

Senecal A, Munsky B, Proux F, Ly N, Braye FE, Zimmer C, Mueller F, Darzacq X. 2014. Transcription factors modulate c-Fos transcriptional bursts. *Cell reports* **8**: 75-83.

Serge A, Bertaux N, Rigneault H, Marguet D. 2008. Dynamic multiple-target tracing to probe spatiotemporal cartography of cell membranes. *Nat Methods* **5**: 687-694.

Sun JM, Chen HY, Espino PS, Davie JR. 2007. Phosphorylated serine 28 of histone H3 is associated with destabilized nucleosomes in transcribed chromatin. *Nucleic Acids Res* **35**: 6640-6647.

Tantale K, Mueller F, Kozulic-Pirher A, Lesne A, Victor JM, Robert MC, Capozi S, Chouaib R, Backer V, Mateos-Langerak J et al. 2016. A single-molecule view of transcription reveals convoys of RNA polymerases and multi-scale bursting. *Nature communications* **7**: 12248.

Tirosh I, Barkai N. 2008. Two strategies for gene regulation by promoter nucleosomes. *Genome Res* **18**: 1084-1091.

Tirosh I, Barkai N, Verstrepen KJ. 2009. Promoter architecture and the evolvability of gene expression. *J Biol* **8**: 95.

Van de Vosse DW, Wan Y, Lapetina DL, Chen WM, Chiang JH, Aitchison JD, Wozniak RW. 2013. A role for the nucleoporin Nup170p in chromatin structure and gene silencing. *Cell* **152**: 969-983.

VanDemark AP, Kasten MM, Ferris E, Heroux A, Hill CP, Cairns BR. 2007. Autoregulation of the rsc4 tandem bromodomain by gcn5 acetylation. *Molecular cell* **27**: 817-828.

Varela I, Tarpey P, Raine K, Huang D, Ong CK, Stephens P, Davies H, Jones D, Lin ML, Teague J et al. 2011. Exome sequencing identifies frequent mutation of the SWI/SNF complex gene PBRM1 in renal carcinoma. *Nature* **469**: 539-542.

Velankar SS, Soultanas P, Dillingham MS, Subramanya HS, Wigley DB. 1999. Crystal structures of complexes of PcrA DNA helicase with a DNA substrate indicate an inchworm mechanism. *Cell* **97**: 75-84.

Verdaasdonk JS, Gardner R, Stephens AD, Yeh E, Bloom K. 2012. Tension-dependent nucleosome remodeling at the pericentromere in yeast. *Mol Biol Cell* **23**: 2560-2570.

Verdin E, Ott M. 2015. 50 years of protein acetylation: from gene regulation to epigenetics, metabolism and beyond. *Nature reviews Molecular cell biology* **16**: 258-264.

Vleeshouwer-Neumann T, Phelps M, Bammler TK, MacDonald JW, Jenkins I, Chen EY. 2015. Histone Deacetylase Inhibitors Antagonize Distinct Pathways to Suppress Tumorigenesis of Embryonal Rhabdomyosarcoma. *PLoS One* **10**: e0144320.

Wang Y, Kallgren SP, Reddy BD, Kuntz K, Lopez-Maury L, Thompson J, Watt S, Ma C, Hou H, Shi Y et al. 2012. Histone H3 lysine 14 acetylation is required for activation of a DNA damage checkpoint in fission yeast. *The Journal of biological chemistry* **287**: 4386-4393.

Wang Z, Zang C, Rosenfeld JA, Schones DE, Barski A, Cuddapah S, Cui K, Roh TY, Peng W, Zhang MQ et al. 2008. Combinatorial patterns of histone acetylations and methylations in the human genome. *Nature genetics* **40**: 897-903.

Whitehouse I, Flaus A, Cairns BR, White MF, Workman JL, Owen-Hughes T. 1999. Nucleosome mobilization catalysed by the yeast SWI/SNF complex. *Nature* **400**: 784-787.

Xue Y, Canman JC, Lee CS, Nie Z, Yang D, Moreno GT, Young MK, Salmon ED, Wang W. 2000. The human SWI/SNF-B chromatin-remodeling complex is related to yeast rsc and localizes at kinetochores of mitotic chromosomes. *Proc Natl Acad Sci U S A* **97**: 13015-13020.

Yen K, Vinayachandran V, Batta K, Koerber RT, Pugh BF. 2012. Genome-wide nucleosome specificity and directionality of chromatin remodelers. *Cell* **149**: 1461-1473.

Zhang Y, Smith CL, Saha A, Grill SW, Mihardja S, Smith SB, Cairns BR, Peterson CL, Bustamante C. 2006. DNA translocation and loop formation mechanism of chromatin remodeling by SWI/SNF and RSC. *Mol Cell* **24**: 559-568.

Zhen CY, Tatavosian R, Huynh TN, Duc HN, Das R, Kokotovic M, Grimm JB, Lavis LD, Lee J, Mejia FJ et al. 2016. Live-cell single-molecule tracking reveals co-recognition of H3K27me3 and DNA targets polycomb Cbx7-PRC1 to chromatin. *Elife* **5**.

Zhu B, Gates LA, Stashi E, Dasgupta S, Gonzales N, Dean A, Dacso CC, York B, O'Malley BW. 2015. Coactivator-Dependent Oscillation of Chromatin Accessibility Dictates Circadian Gene Amplitude via REV-ERB Loading. *Molecular cell* **60**: 769-783.

Figure Legends

Figure 1: Spatial and temporal analysis of global PBAF chromatin binding events using SPT. A. PBAF localization events within the nucleus of a U2-OS cell stably expressing Halo-fBAF180WT. Nuclear envelope is outlined in yellow. Scale bar = 2 μm. B. i. Particle centroid location was determined for each frame in the movie. Particles were temporally linked based on constrained diffusion parameters. Centroid location (red X) was determined as the mean of x- and y-positions. Scalebar = 100 nm. ii-iii. Centroid positions for each particle were mapped within the nucleus. Scalebars = 1 μm in ii and 2 μm in iii. C. Spatial positions of tracks are plotted in 2D with residence times (color-coded based on duration) for each track plotted in the third dimension. D. 1−Cumulative Distribution Function Plots (1−CDF) of PBAF bound to chromatin were fitted to a single (gray dashed) or two-component (red solid) exponential decay model. Fitting analysis reveals that PBAF bound to chromatin display two populations (stable and unstable) of residence times. Percentages of the stable and unstable binding populations are listed next to the residence time. E. Mean stable residence times are displayed for cells expressing either wild-type or bromodomain deleted Halo-fBAF180 constructs following treatment with 2.5 μM SAHA (N = 37 WT cells and 26 ΔBD cells) or vehicle control (N = 39 WT cells and 17 ΔBD cells) for 24 hours. ****= p-value < 0.0001, n.s.= not significant.

Figure 2: High density heat maps of PBAF chromatin binding events. A. Cell nuclei were mapped based on PBAF binding density (left) with regions of high PBAF binding density in red and regions of low PBAF binding density in blue. Areas of above average PBAF binding density were masked (right). B. Representative 1-CDF plots of residence times for molecules within individual masked regions from panel A (right) were fitted with single (gray dashed) and double (red solid) -exponential functions. C. Stable binding residence times across all subcompartments in representative cell displayed in A

Figure 3: Residence time analysis of individual high-density PBAF chromatin binding regions. A. Stable territorial PBAF residence times for wild-type BAF180 containing PBAF (white bars) and BAF180-ΔBD (gray bars). Gaussian fits of wild-type BAF180 containing PBAF (green line) and BAF180-ΔBD (red line) are provided as well. BAF180WT measurements examined 573 subcompartments in 39 cells, while BAF180-ΔBD measurements examined 174 subcompartments in 17 cells. B. Stable territorial PBAF residence times for wild-type BAF180 containing PBAF in cells that have been treated with 2.5 μM SAHA for 24 hours (gray bars) versus vehicle control (white bars). Gaussian fits for cells treated with SAHA (brown line) versus cells treated with vehicle (pink line) are provided as well. Effects of SAHA treatment were assessed from 571 subcompartments in 37 cells and corresponding vehicle treatment was assessed from 573 subcompartments in 39 cells. Vehicle data shown in B is the same as WT vehicle data shown in A of this figure.

Figure 4: Residence time analysis of PBAF binding within H3.3 marked euchromatin versus HP1α marked heterochromatin. A. Cell nuclei were mapped based on H3.3 binding density. Areas of above average H3.3 binding density within the cell were masked (top left, orange). In addition, PBAF binding events within the same cell (top right panel and bottom panel red spots), were mapped within H3.3 subcompartments (bottom, panel orange). B. Stable PBAF residence times within H3.3 (white bars)/HP1α (black bars) subcompartments. Gaussian fits of PBAF binding events within H3.3 (white line) or HP1α (black line) are provided. H3.3 data was amassed from 144 subcompartments within 16 cells and HP1α was amassed from 114 subcompartments within 16 cells.

Figure 5: Clustering analysis of PBAF chromatin binding events. A. PBAF binding density when rastering a 2x2-pixel box across the nucleus. Increased resolution reveals areas of higher

PBAF binding density relative to rastering with an 18x18-pixel box as in Figure 2. B. Global WT PBAF chromatin binding maps were filtered based on duration of binding. Chromatin binding events lasting longer than 2 seconds are shown (red dots). Clustering analysis algorithms revealed repeated PBAF binding events within small foci outlined in blue. Bottom right: Expanded inset of boxed region in top panel demonstrating clustering of PBAF binding events (red dots) within clusters (blue lines). C. Global WT PBAF chromatin binding maps were filtered based on duration of binding. Chromatin binding events lasting longer than 12 seconds are shown (Top left panel, red dots). Simulated PBAF chromatin binding maps (Top right panel, red dots) were generated by randomizing the positions of the filtered binding events within the nucleus. Clustering analysis algorithms revealed repeated PBAF binding events within small foci outlined in blue. Bottom panels: Expanded insets of boxed regions in top panels demonstrating clustering of PBAF binding events (red) within clusters (blue lines).

Figure 6: Analysis of acetylation and bromodomain dependent clustering of PBAF binding to chromatin. A-B. Linear regression of wild-type (blue points and line) or bromodomain deleted (red points and line) BAF180 containing PBAF clusters versus total PBAF tracks at 2- (A) or 8-second (B) event duration filters. C-E. Linear regressions for wild-type BAF180 containing PBAF versus total PBAF tracks at 2- (C), 8- (D), and 12-second (E) event duration thresholds following SAHA (green data points and line) or DMSO (blue data points and line) treatment.

Figure 7: Model of bromodomain dependent effects on PBAF and PBAF binding within transcriptionally active euchromatic regions versus heterochromatic regions. A. Increases in histone acetylation through SAHA treatment leads to an increase in the number of regions that experience re-visiting by the PBAF chromatin remodeling complex. Residence times also increase as shown through our territorial binding analysis. B. PBAF resides in H3.3-rich euchromatin for a shorter duration of time than within HP1α-rich heterochromatin.

Figure 1.

A Single molecule imaging of PBAF in live U2OS cells

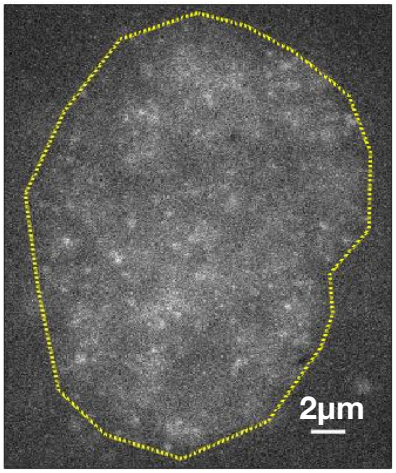

B Localization of PBAF binding events

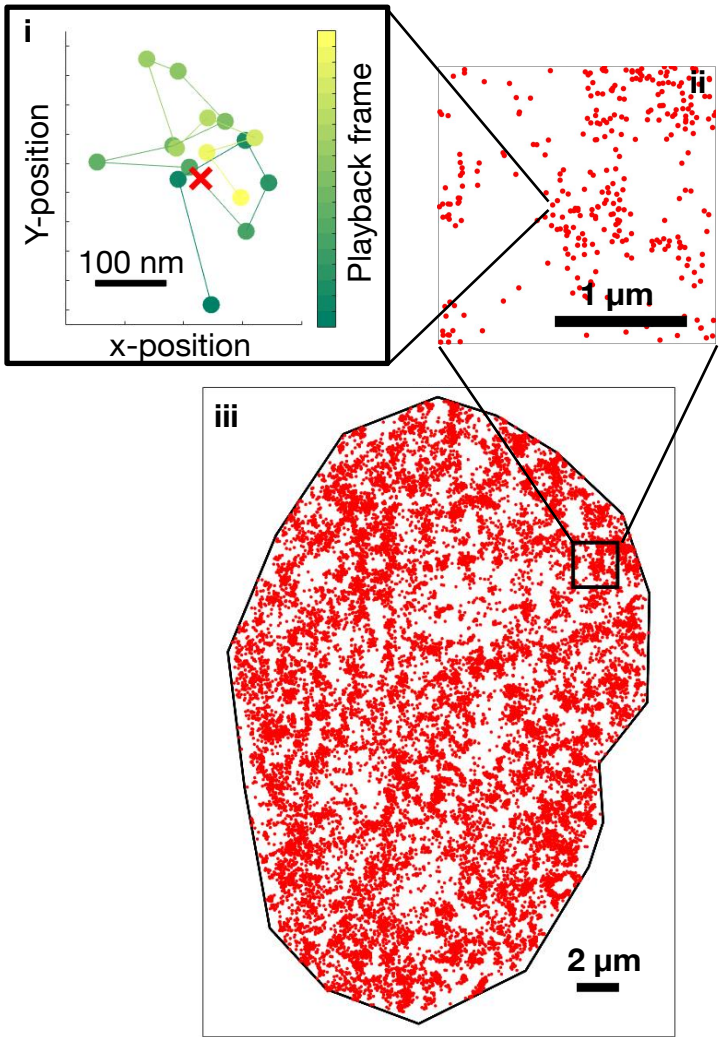

C Residence time of PBAF binding events

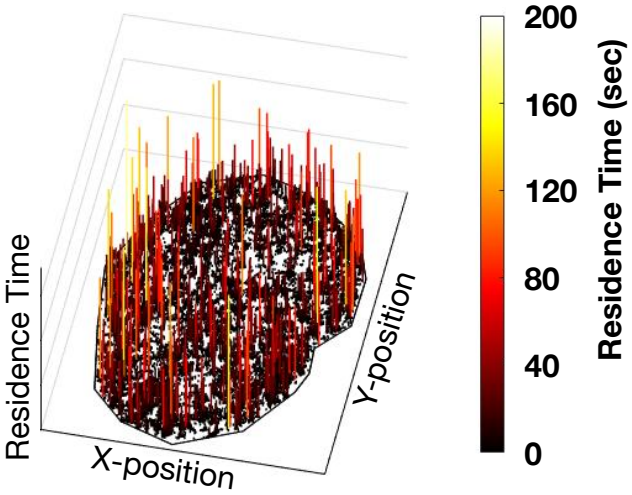

D Probability distribution of PBAF residence time

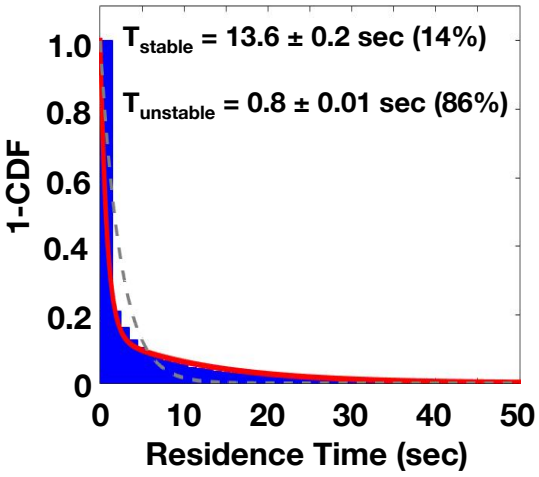

E

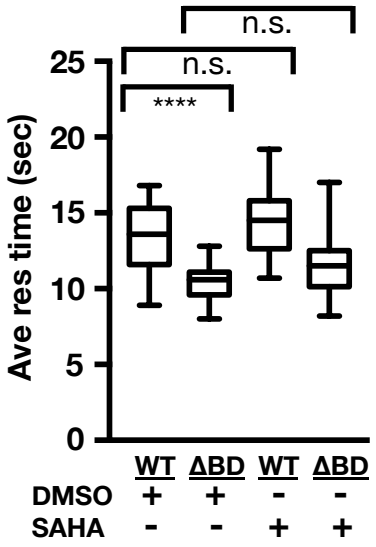

Figure 2

Kenworthy et al_Fig. 2

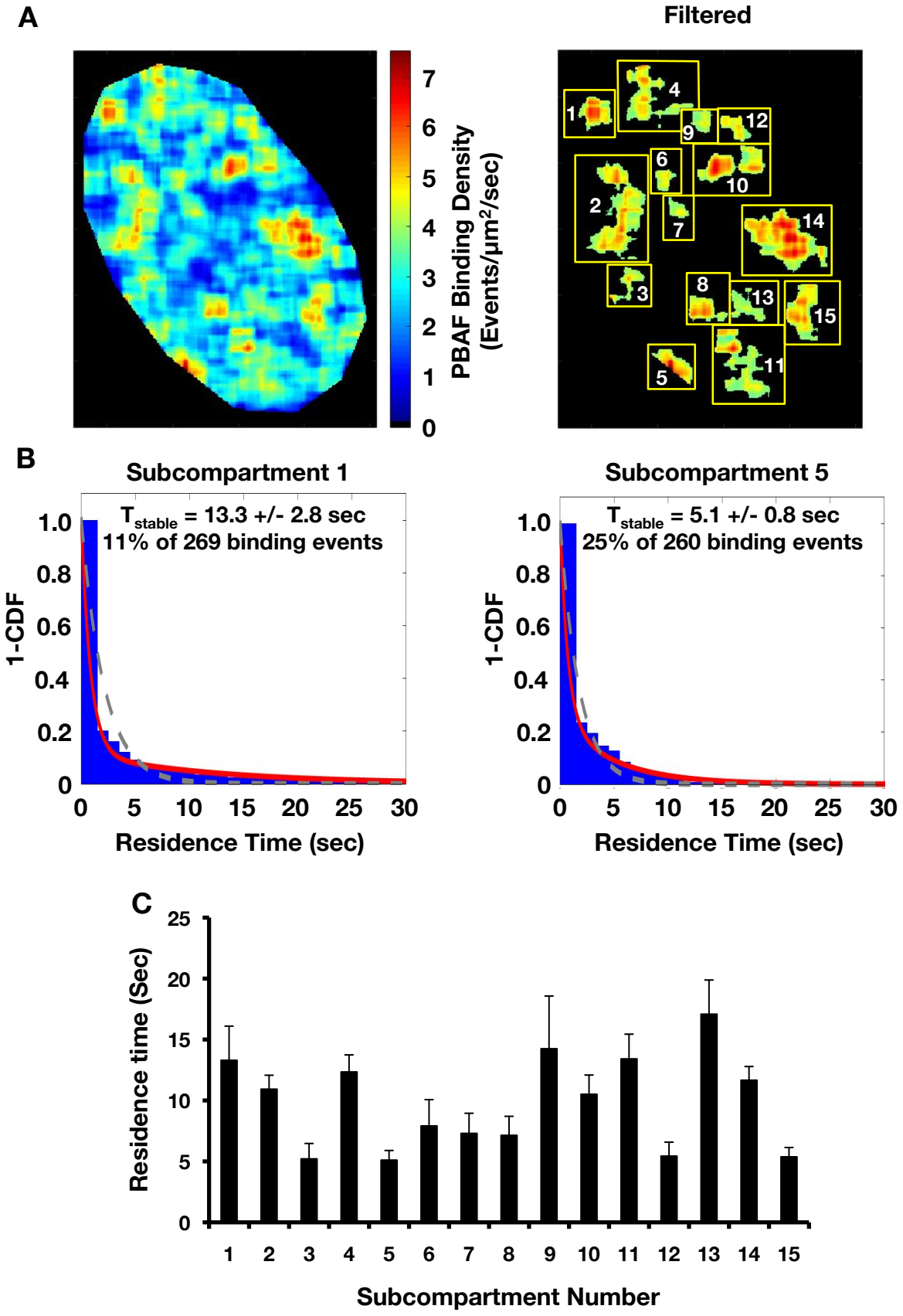

Figure 3

Kenworthy et al_Fig. 3

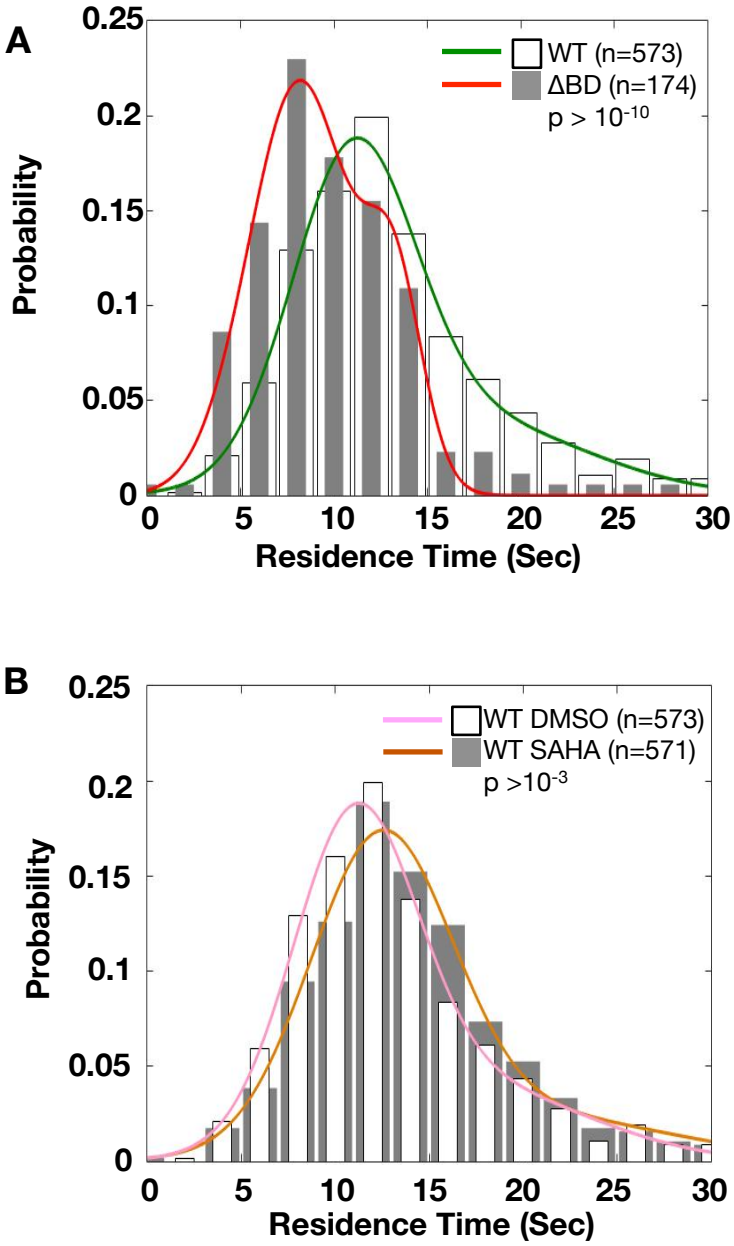

Figure 4

Kenworthy et al_Fig. 4

A

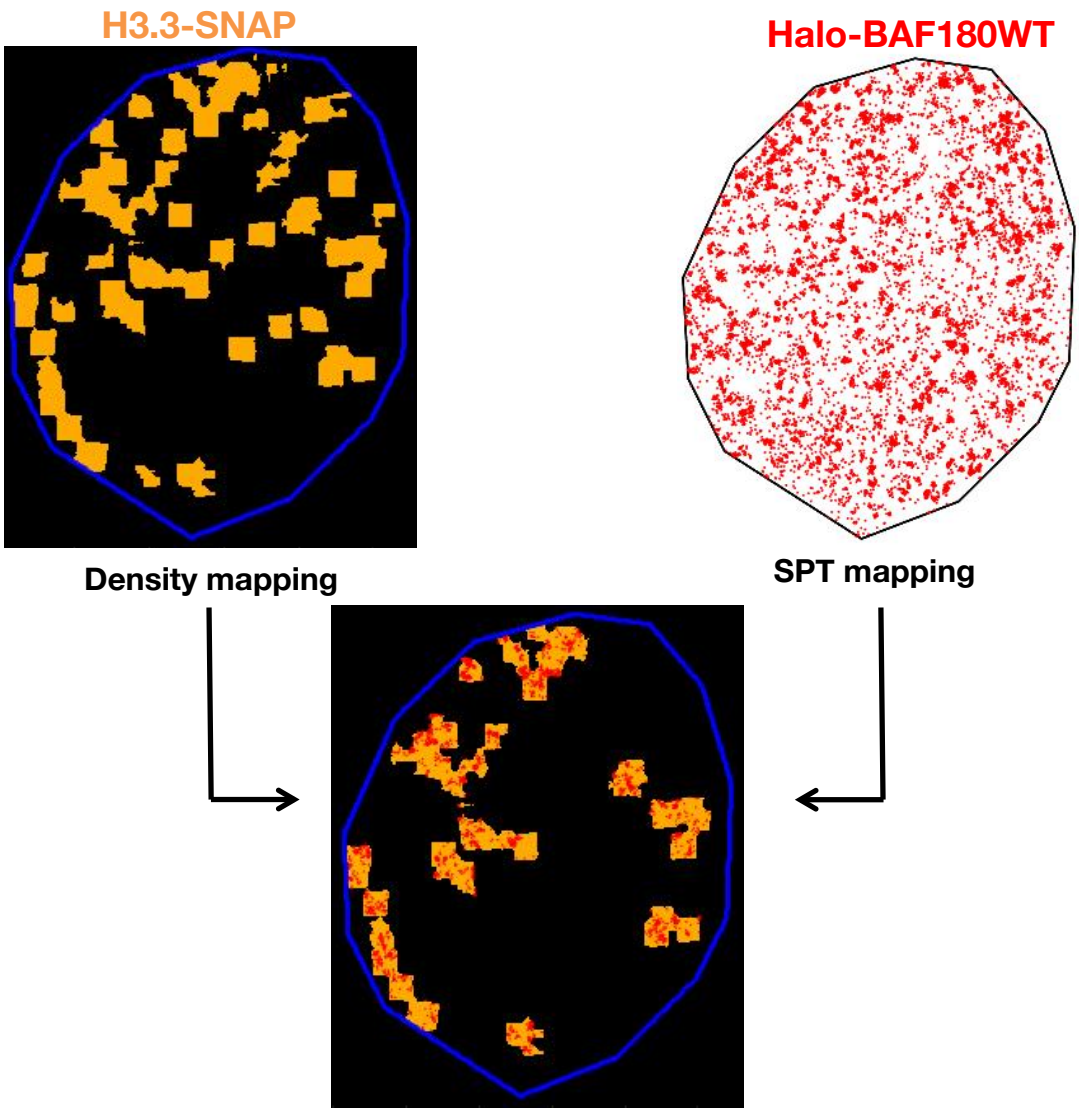

Halo-BAF180WT binding events within H3.3-SNAP subcompartments and SPT characterization.

B

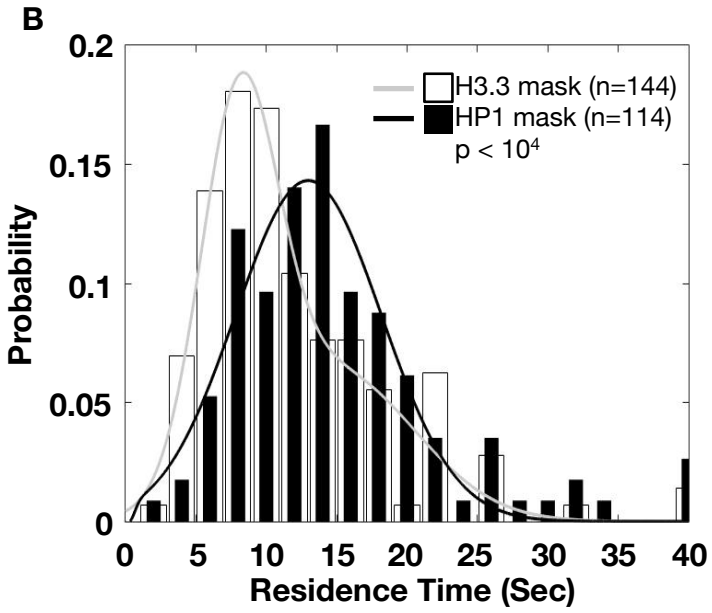

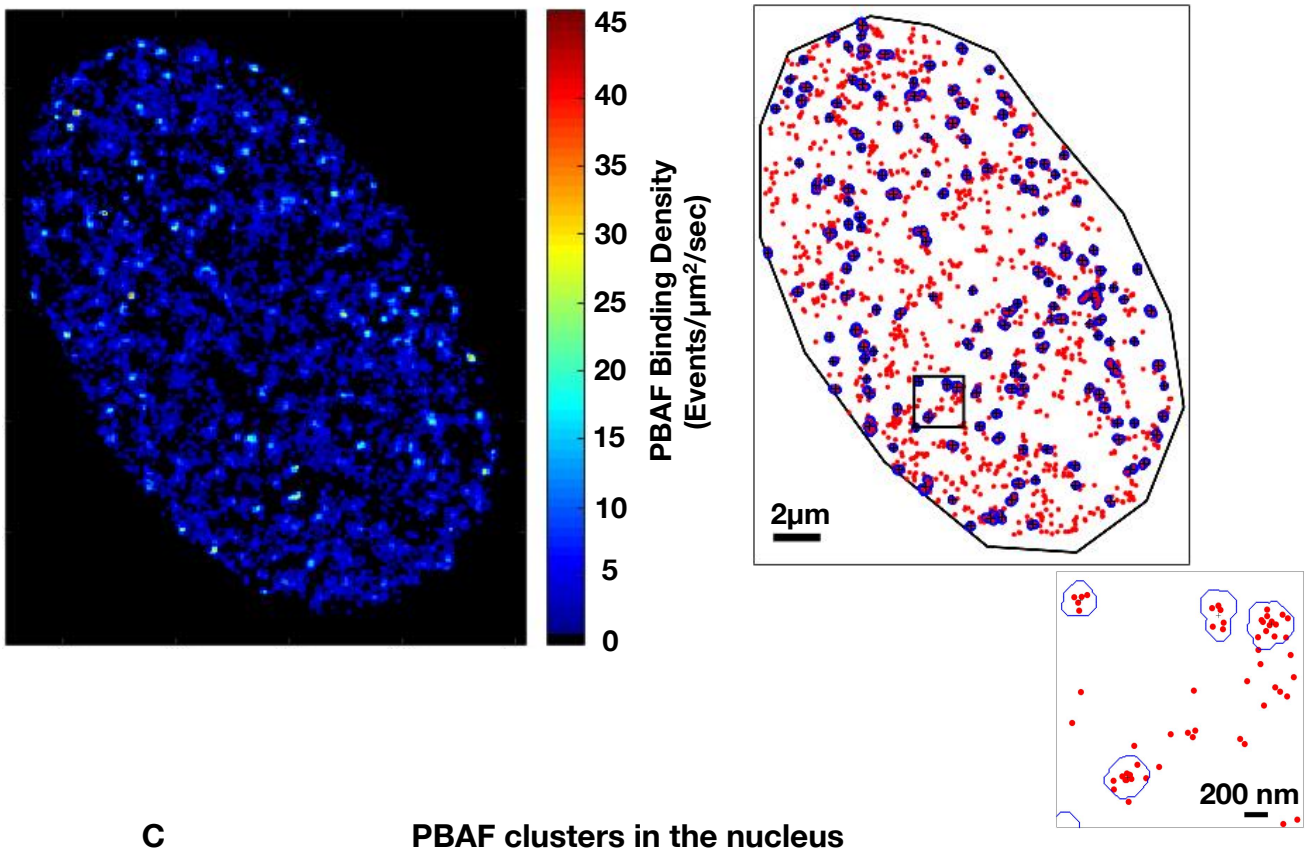

Figure 6

Kenworthy et al_Fig. 6

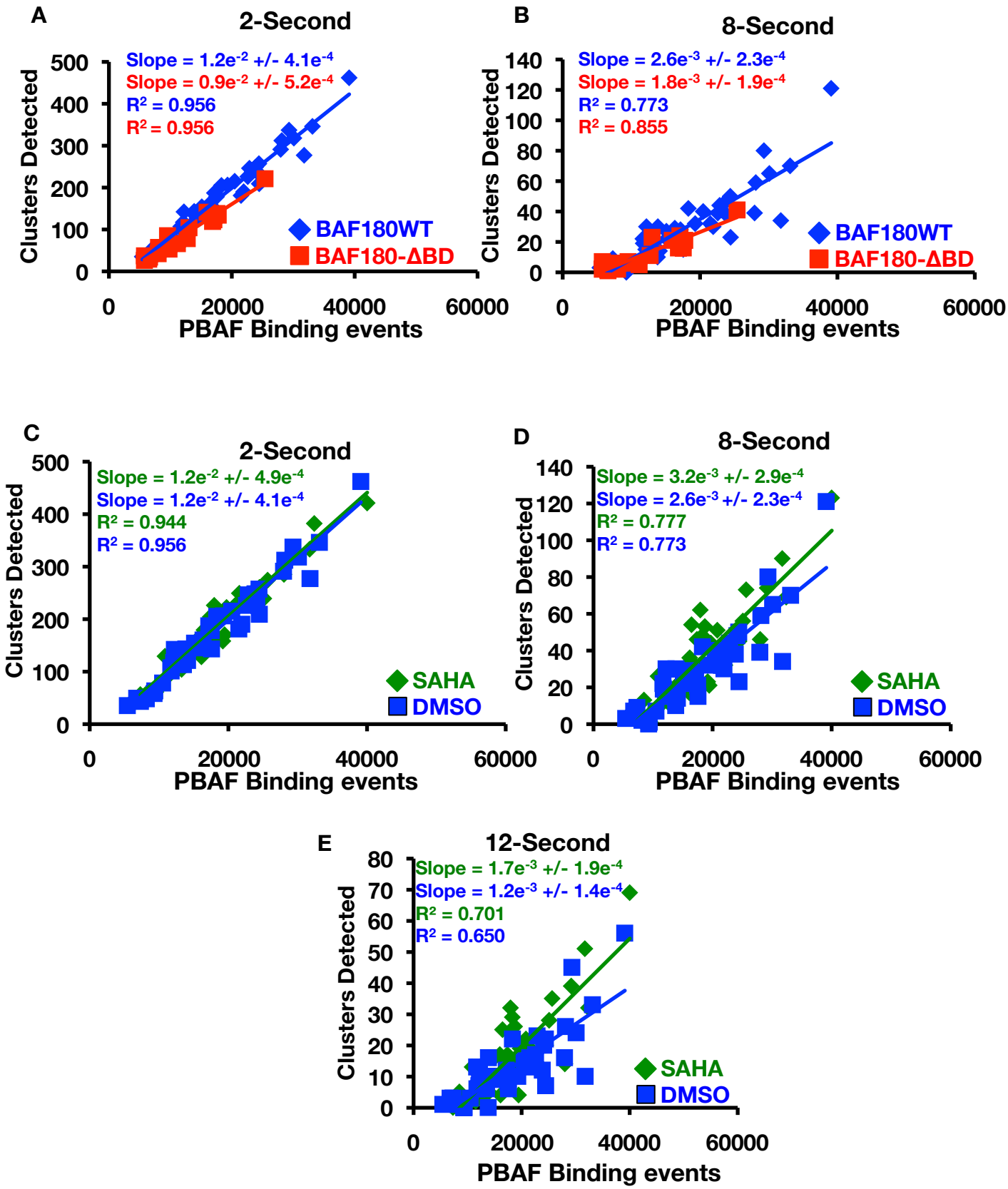

Figure 7

Kenworthy et al_Fig. 7